

Towards energy resolution at the statistical limit from a negative ion time projection chamber

Peter Sorensen^a, Mike Heffner^a, Adam Bernstein^a, Josh Renner^{a,b,c}, Melinda Sweany^a

^aLawrence Livermore National Laboratory, 7000 East Ave., Livermore, CA 94550, USA

^bLawrence Berkeley National Laboratory, 1 Cyclotron Road, Berkeley, CA 94720, USA

^cDepartment of Physics, University of California, Berkeley, CA 94720, USA

Abstract

We make a proof-of-principle demonstration that improved energy resolution can be obtained in a negative-ion time projection chamber, by individually counting each electron produced by ionizing radiation.

Keywords: double beta decay, negative ion, time projection chamber

1. Introduction

Double beta decay is a rare nuclear decay mode, with a typical mean lifetime $\tau > 10^{19}$ y. It was recently observed in ^{136}Xe with a half-life $\tau = 2 \times 10^{21}$ y [1, 2]. The zero neutrino mode of this decay, $\beta\beta(0\nu)$, appears theoretically possible given that neutrinos have non-zero mass. Such a decay would violate lepton number conservation and confirm the Majorana nature of the neutrino. It has not been observed, despite significant ongoing experimental effort world-wide. As in any rare-event search, substantial reduction of radioactive backgrounds are a high priority in the search for $\beta\beta(0\nu)$. Given that the spectral expectation for $\beta\beta(0\nu)$ is a sharp peak at the double beta decay Q-value, excellent energy resolution can be used as an effective discriminant against those backgrounds which remain. But even in the absence of any radioactive background, the sensitivity of a search for $\beta\beta(0\nu)$ may be limited by the high energy tail of the spectrum from the two neutrino decay mode, via the finite energy resolution of the detector. The fraction of $\beta\beta(2\nu)$ counts which contaminate the $\beta\beta(0\nu)$ signal region is given by [3]

$$F = \frac{kQ\delta^6}{m_e} \quad (1)$$

where m_e is the electron mass, $Q = 2458$ keV is the endpoint energy of the decay, δ is the FWHM energy resolution at the endpoint and k is a coefficient which depends

weakly on δ . As an example, suppose a xenon detector obtains $\delta = 0.05$ (equivalently, a Gaussian $\sigma = 2.1\%$). From [3], we find $k = 7$. In a 20 tonne-year exposure (typical of a next generation experiment such as LZ20 [4]), 15 $\beta\beta(2\nu)$ background events would be expected in the $\beta\beta(0\nu)$ signal region. Larger values of δ quickly lead to larger leakage. Only upper limits on the half-life for $\beta\beta(0\nu)$ exist at present. This suggests that there is a significant motivation for developing a new type of xenon detector whose energy resolution approaches the statistical limit.

In this work we make a proof-of-principle demonstration that improved energy resolution can be obtained by individually counting each electron produced by ionizing radiation. The idea has been previously suggested [5, 6] but to our knowledge never implemented. Our detector is a negative ion time-projection chamber, shown schematically in Fig. 1. Rather than drift and detect the electrons created by ionizing radiation, we introduce oxygen as an electronegative dopant to capture the electrons. Oxygen ions O_2^- , rather than electrons, are then drifted to the anode. Just prior to arrival at the anode, the electrons are recovered from the O_2^- and amplified, using a large electron multiplier (LEM) [7]. Ideally, each electron is then individually counted.

The dopant concentration and gas density are tuned so that electron capture occurs over a range of $\sim\text{cm}$. We note that previous negative ion time-projection chambers have used either pure carbon disulfide (CS_2) [8], mixtures of CS_2 with noble gases [9, 10] or nitromethane (CH_3NO_2) [11] dopant. In this work, we employed a mixture of argon (66%, as a low-cost sur-

Email addresses: pfs@llnl.gov (Peter Sorensen), mheffner@llnl.gov (Mike Heffner)

rogate for xenon), carbon dioxide (30%, as quench gas [12]) and oxygen (4%) as electronegative dopant.

2. Apparatus

The construction of our detector is shown schematically in Fig. 1. An enlarged view of the region around the LEM is also shown, with a simulated electron avalanche of gain $\times 30$. The LEM was constructed from copper-clad G10 printed circuit board of thickness 0.432 mm with 0.305 mm diameter holes. After drilling, a chemical etch was used to remove 0.023 mm of copper from the circumference of each hole, in order to increase the breakdown voltage. A segmented anode consisted of four concentric rings of radius 3, 6, 9 and 40 mm, with 0.25 mm standoff between rings. Signals were digitized from the center three anodes, and the large outer ring was simply maintained at ground potential. The rings were used as veto to ensure complete collection of all electrons from each event.

A charge-sensitive preamplifier with a gain of 1.4 V pC^{-1} and recovery time constant $\tau = 140 \text{ } \mu\text{s}$ was connected to each ring, and the calibration was verified by introducing a 10 mV voltage step across a 1 pF capacitance at the preamplifier input. Prior to introducing O_2 dopant, we first verified proper detector operation and LEM gain under electron drift conditions in Ar (with 30% CO_2 quench gas). The $E = 5.9 \text{ keV}$ gammas from the ^{55}Fe source produce $n_0 \equiv E/w = 209$ electrons, based on $w = 28.2 \text{ eV}$. This value was obtained from a weighted average of the argon ($w = 26.3 \text{ eV}$) and CO_2 ($w = 32.8 \text{ eV}$) constituent w -values [14], a result which is confirmed experimentally [15]. These drift as a swarm to the anode, are amplified by the LEM and in the absence of O_2 result in a single, fast output pulse from the preamplifier. Typical pulse rise times were measured to be $O(10) \text{ ns}$. From the known quantities of initial and measured charge, the total effective LEM gain was determined. This is discussed further in Sec. 3. A flow-through system with proportional-integral-derivative feedback pressure regulation was used to mitigate detrimental effects due to detector component out-gassing. Research-grade gas mixtures were used, and stable operation was observed on a timescale of several days. All results presented in this article were obtained at a gas pressure $P = 0.250 \pm 0.001 \text{ bar}$ and $T = 296 \pm 1 \text{ K}$.

There are three distinct regions of electric field in the detector: (i) the $z_d = 110 \text{ mm}$ drift region, with $E_d \sim 0.05 \text{ kV cm}^{-1}$, (ii) the $z_A = 0.432 \text{ mm}$ electron avalanche region E_A in the LEM holes, with typical maximum electric fields of several tens of kV/cm

[16] and (iii) the $z_i = 2 \text{ mm}$ signal induction region, with $E_i = 1 \text{ kV/cm}$. E_A is a function of radial displacement from the center of a hole. Values quoted in this work are given simply by $E_A = \Delta V/z_A$, where ΔV is the bias voltage across the LEM. The high electric field E_A also provided the requisite energy to detach a captured electron from O_2^- . The mechanism for this detachment process is thought to be collisional [17].

The amount of oxygen dopant required to fully capture all electrons created by 5.9 keV photons was first obtained from the measured reduction in pulse height, using electron drift operation. We found that 1% O_2 was sufficient to fully capture all electrons (though higher gas pressures required lower O_2 concentrations). However, the capture probability was sufficiently low that the resulting negative ion signal was distributed across about 10 ms. We found that with 4% O_2 , the resulting signal was localized to within about 5 ms due to the more rapid capture of ionized electrons. This gave an average $22 \text{ } \mu\text{s}$ between subsequent ion arrival times at the LEM, sufficient to allow most ions to generate a distinct signal at the readout plane. In Sec. 4.1 we quantify the fraction of missed ion pulses due to the proximity in time of successive pulses. In order to ensure negligible event pileup, the ^{55}Fe source rate was set at about 3 Hz, using a 0.88 mm diameter collimator.

3. Data acquisition and analysis

3.1. Data acquisition

Negative ion drift event records of 25 ms each were acquired at 20 MHz, with 12-bit vertical resolution. A typical event obtained with an effective LEM gain of 3×10^4 ($\Delta V = 880$ across the LEM) is shown in Fig. 2. Note that effective LEM gain refers to the total observed electron gain from a single electron, and accounts for any reduction due to secondary electrons which did not reach the anode. The interesting portion of the event as digitized is shown in the lower panel. An enlarged view with the effect of the charge preamplifier decay time removed is shown in the upper panel. A total of $n_e = 157$ charge pulse steps were counted: 103 on the center anode, 54 on the adjacent ring anode and 0 on the outer ring anode (not shown). Each step is interpreted as corresponding to a single electron that was recovered from an O_2^- ion, and amplified by the LEM. The possibility of pileup is discussed in Sec. 4.1.

3.2. Analysis algorithm

Our analysis algorithm employs a simple edge-detection scheme: for a given sample i , the average

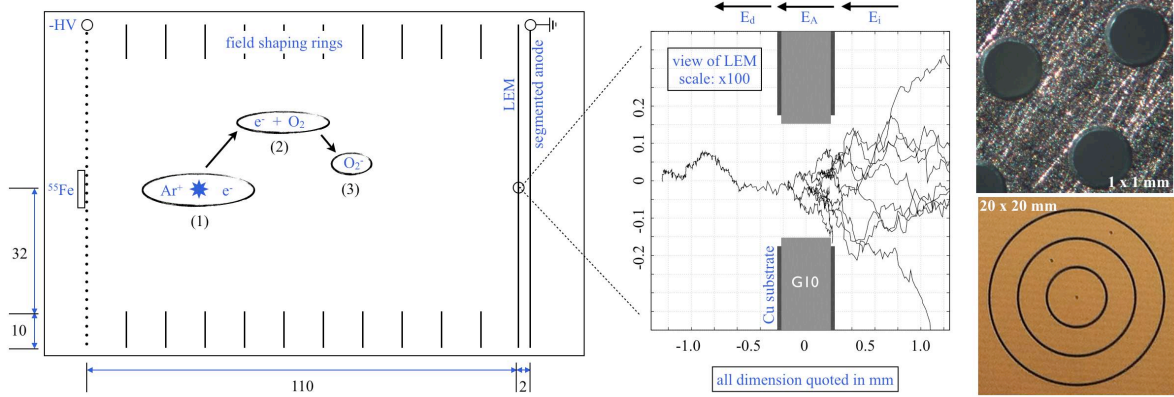


Figure 1: **(Left)** Cross-section schematic of the detector, showing (1) initial generation of electron-ion pairs, (2) rapid electron capture on oxygen and (3) negative ion drift. **(Center)** Enlarged cross-section schematic of the LEM, showing a simulated electron avalanche (with gain $\times 30$) as obtained from the Garfield software [13]. **(Right)** Close-up photographs of the LEM (top) and segmented anode (bottom).

value of the preceding n_b samples are subtracted from the average value of the following n_a samples. The analysis shown in this paper used $n_a = n_b = 10$ samples. As might be expected, increasing the number of samples contained in the average results in a higher signal to noise ratio, allowing smaller pulses to be discerned. We found as many as 5% more pulses with $n_a = n_b = 50$ samples. However, this comes at the expense of also increasing the number of pulses lost to pileup. In other words, the algorithm cannot resolve two single electron pulses that are separated in time by $< n_s/f_{ADC} = 1 \mu\text{s}$. In this equation, $n_s = n_a + n_b$ is the number of samples used to find the edge of a single electron pulse and $f_{ADC} = 20 \text{ MHz}$. These pileup losses could be easily recovered by increasing f_{ADC} .

The algorithm is capable of finding arbitrarily small pulses in an event record. In order to make a meaningful determination of the number of recovered electrons, a pulse height threshold must be chosen. A simple choice is the pulse height value at which the slope of the distribution abruptly steepens, as indicated by the arrow in Fig. 3 (inset). This point corresponds to the onset of spurious noise pulses, and is determined by the input capacitance to the preamplifier. Accordingly, slightly higher thresholds were required on the larger-area anodes. We note that Fig. 3 corresponds to the center anode. The thresholds employed in this analysis were [0.32 0.35 0.42] mV, for the center, ring and outer ring anodes. We also investigated a threshold determination based on the observed pulse height distribution in a region where no signal is present, such as the initial ~ 1 ms of an event record. Both methods lead to similar results.

Additionally, we explored a slightly more sophisti-

cated analysis algorithm in which the existence of a pulse in the event record was determined by the 2nd derivative of the raw event record. In other words, a pulse was identified by a zero-crossing in the double differential. As with the simple scheme, the pulse candidate was still required to pass a threshold requirement. Similar results were obtained with both algorithms.

We note that the analysis avoids double-counting an electron pulse which may have had its signal split across two adjacent rings. This scenario was found to occur on approximately 5% of pulses.

3.3. Single-electron pulse height distribution

Figure 3 shows the distribution of single electron pulse heights corresponding to the conditions exemplified in Fig. 2. The distribution of pulse heights resulting from avalanche multiplication is expected to be exponential [18] and is often referred to as a Furry distribution. We observe a steeper rise at small pulse heights. The origin of this effect is a displacement of the z coordinate at which an electron avalanche was initiated.

Consider the enlarged view of the LEM avalanche region shown in Fig. 1. In that example, the avalanche initiates at $z \approx -0.15 \text{ mm}$. In the absence of O_2^- (electron drift), the variation in the z coordinate of avalanche initiation is $\sigma \approx 0.05 \text{ mm}$, as determined from our detachment model (described in the appendix). When O_2^- is introduced, avalanches are (on average) initiated farther into the LEM, because electrons must first be detached from O_2^- ions. This lowers the effective gain for a majority of electrons, as reflected in the reduced pulse height. This result is confirmed by our detachment model. A simulated pulse height spectrum obtained from the de-

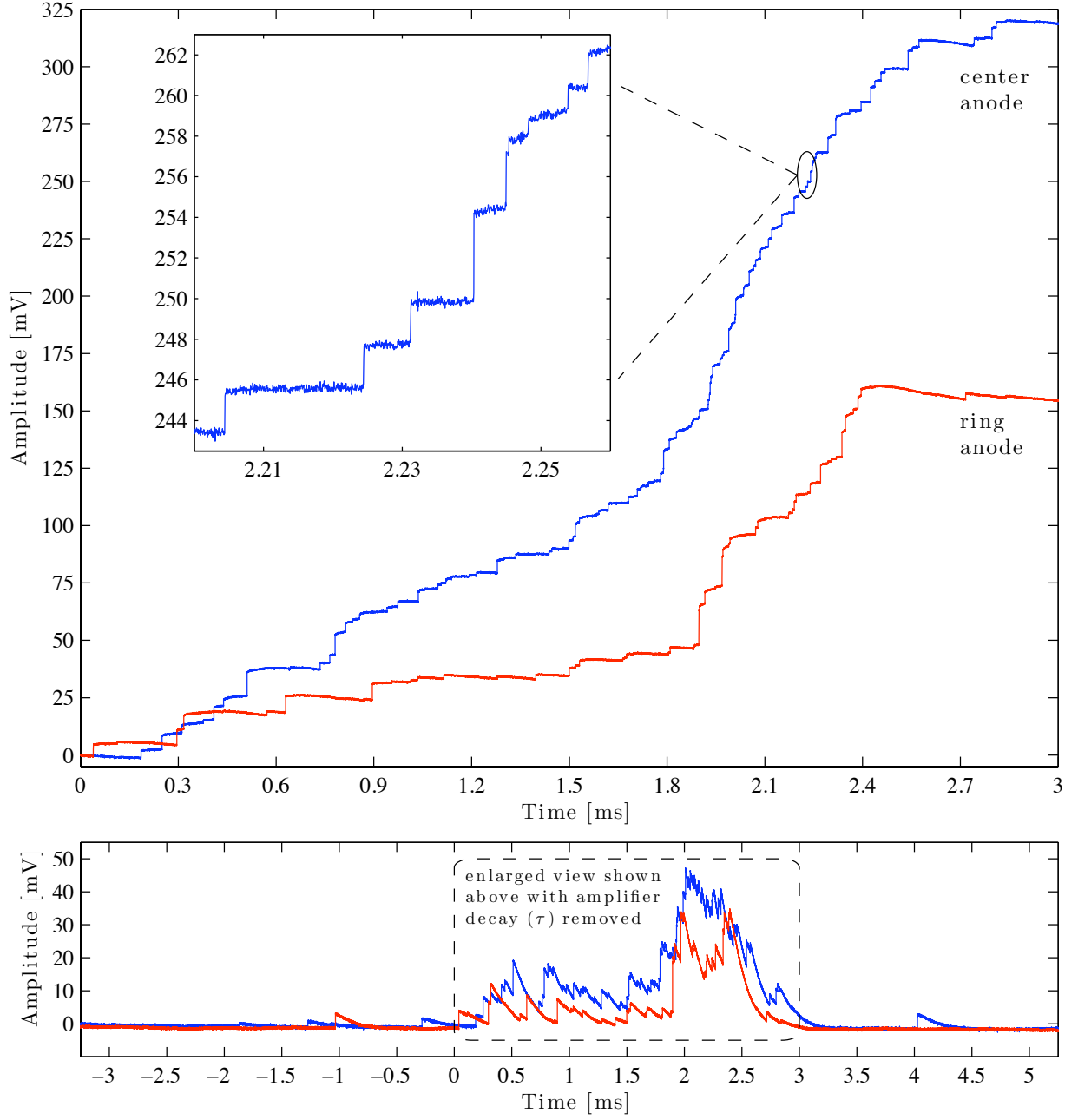


Figure 2: Example event record from 5.9 keV energy deposition in Ar-CO₂ with 4% O₂ dopant at $p = 0.25$ bar. The LEM was operated with $\Delta V = 880$. **(Lower panel)** The event record as digitized. **(Upper panel)** Enlarged view of the event record, after correcting for the charge preamplifier decay constant $\tau = 140 \mu\text{s}$. **(Inset)** Additional detail over a $60 \mu\text{s}$ window.

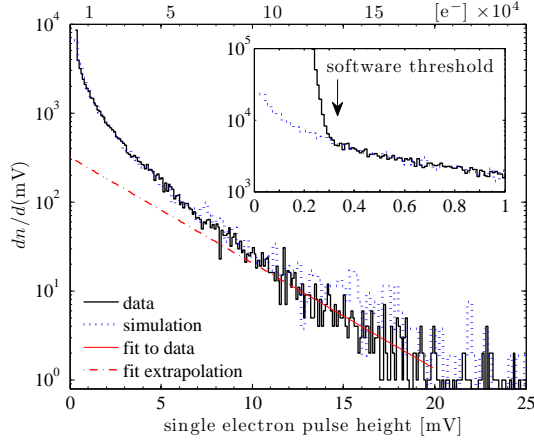


Figure 3: The measured pulse height distribution of single electrons on the center anode, as exemplified in Fig. 2 (black steps). The function $y = \exp(-x/g)$ was fit to the tail of the measured distribution (solid red curve, with small- x extrapolation shown dashed). The pulse height distribution obtained from the detachment model is also shown (dotted blue steps). Equivalent effective LEM gain is indicated along the top axis. (**Inset**) The pulse height distribution near pulse detection threshold (< 1 mV).

achment model is also shown in Fig. 3, normalized to the number of counts above the software threshold.

3.4. Gain curves

Gain curves for the LEM are shown in Fig. 4, for 0% (stars) and 4% (circles) O_2 . The addition of O_2 lowers the effective gain at any particular voltage. With 0% O_2 the signal corresponding to the full-energy peak is a single pulse with a fast $O(10)$ ns rise time. The gain curve for 0% O_2 was obtained from that total pulse height, as described in Sec. 2. The curve for 4% O_2 was obtained from fitting $y = \exp(-x/g)$ to the tail of the single electron pulse height distribution, as shown in Fig. 3. The decay constant g of the exponential (in mV) was taken to indicate the mean gain at each voltage. Considering Fig. 3, it is expected that this procedure may result in a modest overstatement of the effective gain. We note that the present work does not require a precise knowledge of the gain; however, it is critical to verify that the gain is sufficiently large to see single electron pulses.

4. Results

A typical energy spectrum obtained from counting recovered single electrons on the center and ring anodes is shown in Fig. 5. Software data selection cuts required ≤ 1 electron pulse in the first and last 3 ms of events, and ≤ 5 electron pulses on the outer ring anode. The energy resolution is discussed in Sec. 4.2.

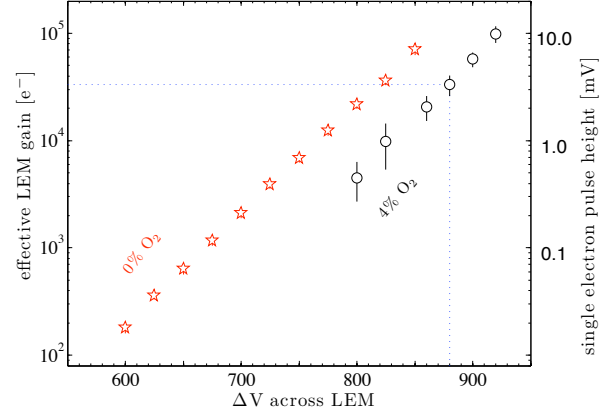


Figure 4: Gain curves for the LEM. The dotted crossed lines indicate the data point corresponding to the examples shown in Fig. 2, Fig. 5 and Fig. 3. Where not visible, uncertainty is smaller than the data point.

4.1. Counting losses

Figure 6 shows the number n_e of counted electrons as a function of LEM bias voltage. A maximum electron counting efficiency of 0.78 was obtained. We consider several likely electron loss mechanisms:

- electrons which were not recovered from O_2^- .
- electrons which were recovered from O_2^- but did not produce an avalanche above threshold.
- electrons which were recovered, produced an avalanche above threshold but were not resolved due to the finite value of f_{ADC} .
- O_2^- ions which collided with the top (in voltage) of the LEM, rather than being directed into one of the multiplication holes.
- “gas-phase chemistry” [6]. An example would be a dissociation reaction which left an appreciable fraction of e.g. O^- , whose higher electron affinity then precludes any hope of recovering the captured electron. Quantifying this effect is beyond the scope of this work, and is not discussed further.

Addressing items (a) and (b), the trend of the data suggests that the full number of initial electrons could be recovered, if only ΔV could be increased by another ~ 50 V. However, in this bias regime frequent electrical breakdown makes the LEM gain structure unusable.

Addressing item (b) in particular, we can use our detachment model to make a rough estimate of the fraction of single electron pulses which were lost below the software threshold. Looking at the simulated curve in Fig. 3 (inset), the predicted fraction of pulse heights below the

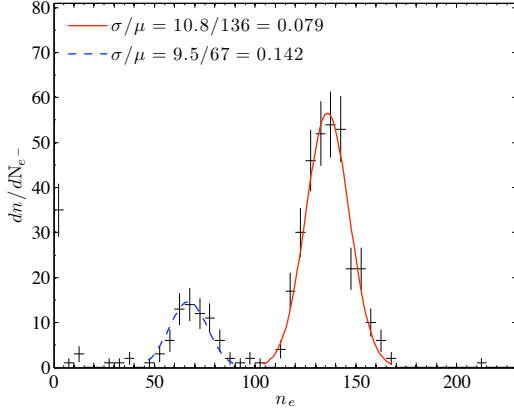


Figure 5: The energy spectrum obtained from counting individual electrons recovered from O_2^- ions, obtained in Ar- CO_2 at $p = 0.25$ bar with 4% O_2 dopant. The LEM was operated with $\Delta V = 880$. The full-energy peak is 5.9 keV and the argon k-shell escape peak is 3.1 keV.

software threshold is about 0.41. Under the experimental conditions shown there ($\Delta V = 880$), the total fraction of electrons not counted was $1 - 136/209 = 0.35$. We see that the model slightly over-predicts the losses below software threshold. This is not surprising since there may be other factors (not addressed by the model) which influence the shape of the pulse height distribution. Nevertheless, the rough agreement is encouraging.

Addressing item (c), the fraction of pulses lost to pileup is approximately $n_c n_s / N$, where n_c is the number of pulses occurring on a channel during the N samples spanning a typical event. As shown in Fig. 2, typically $N \approx 6 \times 10^4$ samples. From Sec. 3.2, $n_s = 20$. We must have $n_c \leq n_e$, where n_e is the total number of pulses in an event. The limiting case occurs if all the electrons arrive at the same channel. Taking $n_c = 136$ as in Fig. 5, this simple estimate implies that the typical maximum fraction of electrons lost to pileup is 0.04. The result is confirmed by a detailed analysis of the time between successive pulses in all events in our data sample.

Addressing item (d), the next obvious parameter which might be increased is the induction field strength E_i . Previous studies [16] have shown that the transparency of a LEM for electrons depends on E_i . For LEM bias values $\Delta V \lesssim 880$, we found that by doubling E_i from 1 kV/cm to 2 kV/cm we obtained a 20% increase in the number of recovered electrons. Further increase of E_i did not yield additional recovered electrons. Interestingly, when operating at higher bias values $\Delta V > 880$ with $E_i = 2$ kV/cm, the maximum number of recovered electrons was still limited to about $\times 0.78$.

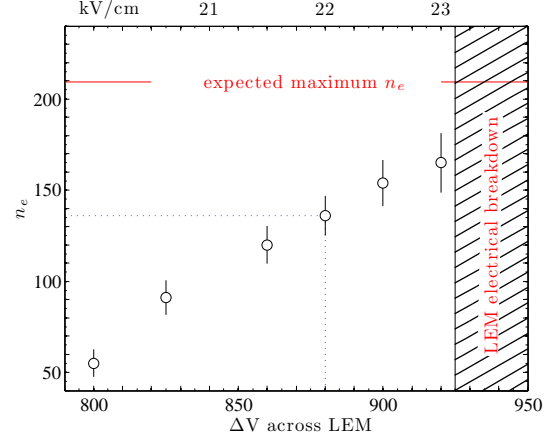


Figure 6: Average number n_e of counted electrons (with 1σ width) as a function of bias voltage ΔV across the LEM. Corresponding $E_A = \Delta V / z_d$ is indicated along the top.

An additional complication of operation at $E_i > 1$ kV/cm is a distortion of the pulse shape. With $E_i = 1$ kV/cm individual pulse shapes were as expected: a voltage step with fast $O(10)$ ns rise time, followed by recovery with $\tau = 140 \mu s$. With $E_i = 2$ kV/cm, we observed the same initial fast rise time, followed immediately by a slow $\sim 3 \mu s$ rise time, followed by recovery with the expected time constant. The step height of the slow rise time was less than half the step height of the fast rise time, and was observed even in the absence of oxygen. This leads to the interpretation that it is due to positive ion movement between the lower (in voltage) electrode of the LEM and the anode. Physically, this implies that the electron avalanche continued for several hundred microns beyond the lower electrode plane of the LEM.

We have assumed that w -value is unaffected by the presence of the oxygen dopant. This seems reasonable since oxygen serves to remove, rather than add, ionized electrons. However, for completeness we note that if the w -value were higher (lower) by *e.g.* 2 eV, the predicted resolution shown in Fig. 7 would be lower (higher) by only a few percent. This is a small effect – roughly equivalent to the line width of the curve. At the same time, the expected maximum n_e shown in Fig. 6 would decrease (increase) by about 7%.

4.2. Energy resolution

The best energy resolution we achieved under electron drift conditions (in the absence of O_2) was $\sigma/\mu = 0.11$. In Fig. 7 we show the energy resolution σ/n_e as a function of n_e , as obtained from negative ion drift.

Statistical uncertainty is indicated by the thin vertical bar, and in several cases is smaller than the data point. Sources of systematic uncertainty, indicated by the larger vertical rectangle, include (1) varying $n_{a,b}$ between 10 and 20 samples, (2) variation due to binning and fitting and (3) differences in results between two independent analyses. The last item implicitly accounts for variation in the determination of the pulse detection software threshold.

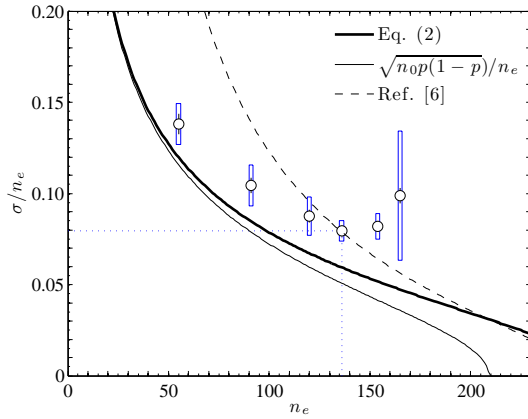


Figure 7: Observed energy resolution (circles) compared with the expectation for a binomial process (thin solid), the prediction from Ref. [6] and our prediction as given by Eq. 2 (thick solid). Statistical uncertainty is indicated by the thin vertical bars, and systematic uncertainty (discussed in the text) is indicated by the vertical rectangles.

The expected detector resolution for electron counting is

$$\sigma/n_e = \sqrt{\frac{F}{n_0} + \frac{(1-p)}{n_0 p}} \quad (2)$$

where $F = 0.20$ [19] is the Fano factor in gaseous argon. This equation states that the resolution depends on the Fano fluctuation in initial number n_0 of ionized electrons, and on the binomial process by which electrons are recovered from O_2^- and amplified. As mentioned previously, we define $n_e = n_0 p$, where p is the total probability for an electron to be counted.

The agreement between Eq. 2 and the data is not satisfactory for any value of n_e . We are therefore lead to consider other processes which remain unaccounted in our analysis. We note that if the measured n_e values were $\sim 30\%$ smaller, our data would appear to agree well with Eq. 2. This leads to the suspicion of a spurious double-counting of recovered electrons. We have already removed the possibility of double-counting pulses across adjacent anodes. There remains the possibility

of double-counting due to some sort of feedback mechanism. For example, we know that copious UV photons are generated during the electron avalanche. Could there be a small probability that one of these photons eject an electron from *e.g.* the wall of the LEM, leading to a spurious electron pulse? We have investigated this possibility and found no concrete evidence to support the hypothesis, but this does not allow us to rule it out. For completeness we note that the discrepancy we observe cannot be accounted for by any reasonable variation in the Fano factor. We also note that our data do not support the theoretical energy resolution proposed in [6].

5. Summary and future work

We have demonstrated that improved energy resolution can be achieved in a negative ion time projection chamber by individually counting the electrons produced by ionizing radiation. The initial results are encouraging, but many questions remain to be addressed. Higher electron gain and a higher electric field E_A are clear priorities. Future work will study the electron counting performance using proportional wire and MICROMEGAS gain structures, as well as optimal gas mixtures (including our desired target isotope, xenon) and operation at increased gas pressure.

Appendix: a simplified electron detachment model

In order to further understand the physics underlying the single electron pulse height distribution discussed in Sec. 3.3, we employed a simplified model of the detachment process. It was assumed that O_2^- ions drift in an ideal gas of neutral argon molecules in thermal equilibrium. The ions make elastic collisions described by a cross section calculated assuming a long-range polarization interaction with the neutral atom [20]. They are accelerated by a constant electric field between collisions. The electron detaches from the ion when the center of mass energy of the ion-neutral system (between collisions) exceeds a threshold ϵ_D . Using momentum transfer theory [21], the model produced a lifetime for electron detachment for a given electric field strength and ϵ_D , and a distribution of detachment probabilities for a given electric field profile. It would seem natural to associate ϵ_D with the electron affinity, which is $\epsilon = 0.45$ eV [22] for O_2 . Based on experimental determinations of the collision cross section for detachment of both O_2^- ions [23] and several types of halogen ions [24], it appears that ϵ_D can often exceed the electron affinity by $\times 2$ or more.

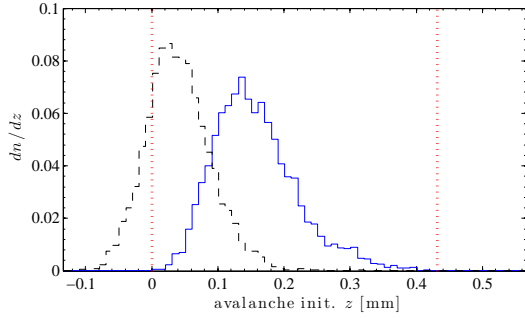


Figure 8: Simulated distribution of z coordinate at which electron avalanches begin, with (solid) and without (dashed) O_2 . The vertical dotted lines indicate the physical extent of the LEM.

We therefore treated ε_D as a free parameter. Different values of ε_D resulted in different z detachment profiles. These were incorporated into Monte Carlo simulation to study the effects of ion detachment on single-electron pulse height distributions. The simulated pulse height distribution for the avalanche gain for $\varepsilon_D = 3$ eV is shown in Fig. 3. The point of avalanche initiation which resulted from the detachment profile (also obtained with $\varepsilon_D = 3$ eV) is shown in Fig. 8. The results were obtained for a gas mixture of $ArCO_2$, using Garfield++ [25] in conjunction with Gmsh [26] and Elmer [27]. The simulated distribution for electron drift is also shown. We note that by default, the predicted gain was about $\times 10$ too low. This may be partially due to Penning processes which are not accounted for in the Garfield++ simulation [28]. As an interim solution we explored the effect of varying the default Townsend coefficient data input to Garfield++, and found reasonable agreement (as shown here) with a uniform increase of 19%. This is well within the range allowed by experimental uncertainty [29, 30].

Acknowledgments

This work was performed under the auspices of the U.S. Department of Energy by Lawrence Livermore National Laboratory in part under Contract DE-AC52-07NA27344. J. Renner also acknowledges support from the Stewardship Science Graduate Fellowship (grant number DE-FC52-08NA28752). We are indebted to A. Goldschmidt, D. Nygen, J. Siegrist and D. Snowden-Ifft for useful discussions.

References

[1] N. Ackerman *et al.* (EXO Collaboration), Phys. Rev. Lett. **107** 212501 (2011).

[2] A. Gando *et al.* (KamLAND-Zen Collaboration), arXiv:1201.4664 (2012).
[3] S.R. Elliott and P. Vogel, Annu. Rev. Nucl. Part. Sci. **52** 115 (2002).
[4] D.C. Mallin *et al.* (LUX Collaboration), arXiv:1110.0103
[5] C.J. Martoff, R. Ayad, M. Katz-Hyman, G. Bonvicini and A. Schreiner, Nucl. Instr. Meth. A **555** 55 (2005).
[6] D.R. Nygren, J. Phys. Conf. Ser. **65** 012003 (2007).
[7] A. Breskin *et al.*, Nucl. Instr. Meth. A **598** 107 (2009).
[8] C.J. Martoff, D.P. Snowden-Ifft, T. Ohnuki, N. Spooner and M. Lehner, Nucl. Instr. Meth. A **440** 355 (2000).
[9] D.P. Snowden-Ifft, C.J. Martoff and J.M. Burwell, Phys. Rev. D **61** 101301 (2000).
[10] T. Ohnuki, D.P. Snowden-Ifft and C.J. Martoff, Nucl. Instr. Meth. A **463** 142 (2001).
[11] C.J. Martoff, M.P. Dion, M. Hosack, D. Barton and J.K. Black, Nucl. Instr. Meth. A **598** 501 (2009).
[12] A. Bressan, A. Buzulutskov, L. Ropelewski, F. Sauli and L. Shekhtman, Nucl. Instr. Meth. A **423** 119 (1999).
[13] R. Veenhof, <http://garfield.web.cern.ch>.
[14] W. Blum, W. Riegler and L. Rolandi, *Particle Detection with Drift Chambers*, Springer-Verlag, Berlin (2008).
[15] T.E. Bortner, G.S. Hurst, Mildred Edmundson and J.E. Parks, *Alpha particle ionization of argon mixtures – further study of the role of excited states*, Oak Ridge National Laboratory report ORNL-3422 and TID-4500 (1963).
[16] C. Shalem, R. Chechik, A. Breskin and K. Michaeli, Nucl. Instr. Meth. A **558** 475 (2006).
[17] M.P. Dion, C.J. Martoff and M. Hosack, Astropart. Phys. **33** 216 (2010).
[18] A.H. Cookson and T.J. Lewis, Brit. J. Appl. Phys. **17** 1473 (1966).
[19] M. Kase, T. Akioka, H. Mamyoda, J. Kikuchi and T. Doke, Nucl. Instr. Meth. A **227** 311 (1984).
[20] G. Gioumiosis and D. P. Stevenson, J. Chem. Phys. **29** 294 (1958).
[21] E. A. Mason and E. W. McDaniel, *Transport Properties of Ions in Gases* (Wiley, New York, 1988).
[22] K.M. Ervin, I. Anusiewicz, P. Skurski, J. Simons and W.C. Lineberger, J. Phys. Chem. A **107** 8521 (2003).
[23] M. J. Wynn, J. D. Martin, and T. L. Bailey, J. Chem. Phys. **52** 191 (1970).
[24] B. T. Smith, W. R. Edwards, L. D. Doverspike, and R. L. Cham- pion, Phys. Rev. A **18** 945 (1978).
[25] H. Schindler and R. Veenhof *et al.*, Garfield++, <http://garfieldpp.web.cern.ch/garfieldpp>.
[26] C. Geuzaine and J.-F. Remacle, *Gmsh: a three-dimensional finite element mesh generator*, Int. J. Numer. Meth. Eng. **79** 1309 (2009).
[27] *Elmer: Open Source Finite Element Software for Multiphysical Problems*, <http://www.csc.fi/english/pages/elmer>
[28] R. Veenhof, *private communication*.
[29] G. Auriemma, D. Fidanza, G. Pirozzi, C. Satriano, Nucl. Instr. Meth. A **513** 484 (2003).
[30] A. Sharma and F. Sauli, Nucl. Instr. Meth. A **334** 420 (1993).